Nanoscale

PAPER

View Article Online
View Journal

Cite this: DOI: 10.1039/c7nr03026f

Advanced carbon dots *via* plasma-induced surface functionalization for fluorescent and bio-medical applications†

So Young Park,[a] Che Yoon Lee,[a] Ha-Rim An,[a] Hyeran Kim,[a] Young-Chul Lee,[b] Edmond Changkyun Park,[c] Hang-Suk Chun,[d] Hee Young Yang,[d] Sae-Hae Choi,[e] Hee Sik Kim,[e] Kyoung Suk Kang,[f] Hyun Gyu Park,[f] Jong-Pil Kim,[g] Yunju Choi,[g] Jouhahn Lee[a] and Hyun Uk Lee *[a]

Received 28th April 2017,
Accepted 3rd June 2017

DOI: 10.1039/c7nr03026f

rsc.li/nanoscale

Multifunctional carbon-based nanodots (C-dots) are synthesized using atmospheric plasma treatments involving reactive gases (oxygen and nitrogen). Surface design was achieved through one-step plasma treatment of C-dots (AC-paints) from polyethylene glycol used as a precursor. These AC-paints show high fluorescence, low cytotoxicity and excellent cellular imaging capability. They exhibit bright fluorescence with a quantum yield twice of traditional C-dots. The cytotoxicity of AC-paints was tested on BEAS2B, THLE2, A549 and hep3B cell lines. The *in vivo* experiments further demonstrated the bio-compatibility of AC-paints using zebrafish as a model, and imaging tests demonstrated that the AC-paints can be used as bio-labels (at a concentration of <5 mg mL^{-1}). Particularly, the oxygen plasma-treated AC-paints (AC-paints-O) show antibacterial effects due to increased levels of reactive oxygen species (ROS) in AC-paints (at a concentration of >1 mg mL^{-1}). AC-paints can effectively inhibit the growth of *Escherichia coli* (*E. coli*) and *Acinetobacter baumannii* (*A. baumannii*). Such remarkable performance of the AC-paints has important applications in the biomedical field and environmental systems.

Introduction

Currently, photoluminescent carbon-based nanomaterials have been the subject of extensive research in biology, environmentology and energy materials because their optical and chemical properties are similar to those of conventional semiconductor quantum dots (QDs).[1–8] According to previous studies, there has been much research on the potential applications of carbon-based QDs for biomedical applications because these materials are nontoxic, unlike the heavy metal-containing semiconductor QDs.[9–18] For example, Wei *et al.* demonstrated that nitrogen-doped carbon dots displayed a high quantum yield (QY) for tuneable multicolour displays.[19]

We reported a large-scale preparation method to produce C-dots for bio-imaging and photocatalytic performance.[20–22] Despite this, the development of new uses of C-dots as antibacterial agents has not been reported. Antibacterial materials are now widely used to improve public health.[23–27] Other antibacterial materials including silver nanoparticles,[28,29] titanium oxide nanoparticles,[30,31] graphene,[32–34] and carbon nanotubes (CNTs)[35,36] have been found to be cytotoxic; on the other hand, carbon dots have strong fluorescence and do not cause any serious health or environmental problems.[37–39]

Very recently, we introduced liquid-type fluorescent carbon dots (C-paints) by the ultrasound irradiation of polyethylene glycol (PEG).[20] From the perspective of synthesis, it is desirable to mass fabricate C-dots by facile and practical processing. However, it is still rewarding to search for alternative synthetic approaches to achieve improved optical and chemical properties for C-dots. Before that, much study has been carried out *via* surface passivation of C-dots for the improvement of fluorescence, water solubility and toxicity.[2,14,40,41] Based on the above studies, it would be desirable if advanced C-paints could be obtained by a simple adjustment of atmospheric plasma con-

[a]*Advanced Nano-surface Research Group, Korea Basic Science Institute (KBSI), Daejeon 34133, Republic of Korea. E-mail: leeho@kbsi.re.kr*
[b]*Department of BioNano Technology, Gachon University, Gyeonggi-do 13120, Republic of Korea*
[c]*Drug and disease target group, Korea Basic Science Institute (KBSI), Ochang, Cheongju 28119, Republic of Korea*
[d]*Department of Predictive Toxicology, Korea Institute of Toxicology (KIT), Daejeon 34114, Republic of Korea*
[e]*Sustainable Bioresource Research Center, Korea Research Institute of Bioscience and Biotechnology (KRIBB), Daejeon 34141, Republic of Korea*
[f]*Department of Chemical and Biomolecular Engineering (BK21+Program), Korea Advanced Institute of Science and Technology (KAIST), Daejeon 34141, Republic of Korea*
[g]*High Technology Components & Materials Research Center, Korea Basic Science Institute (KBSI), Busan 46742, Republic of Korea*
†Electronic supplementary information (ESI) available. See DOI: 10.1039/c7nr03026f

ditions. Compared with the traditional surface functionalization method of C-dots at high temperature with an additive passivation agent, the atmospheric plasma treatment is advantageous because of its the facile process that does not require any additives at room temperature. In the present study, the reactive gases (O_2 or N_2) in the plasma system were used as oxygen or nitrogen sources to produce various functional groups of C-dots (Table 1).[40–44]

Herein, we present a simple one-step method to prepare large-scale advanced C-paints (AC-paints) by directly applying atmospheric plasma with reactive gas (oxygen and nitrogen) to as-synthesized C-paints. Compared with traditional C-paints, the plasma can generate functional groups on the surface of C-paints, thus enhancing fluorescence efficiency and leading to the enhancement of antibacterial property. The AC-paints can be mass-produced using atmospheric plasma and easily processed to make reactive oxygen species (ROS) on the surface at low cost, which provides a promising insight into their bacterial performance. We expect AC-paints to offer a range of opportunities for the development of biological and antibacterial research. Particularly, the obtained oxygen plasma-treated AC-paints (AC-paints-O) are excellent bio-labelling agents, which can effectively inhibit the growth of *E. coli* and *A. baumannii* cells at low concentration of AC-paints-O (>1 mg mL^{-1}), while showing minimal cytotoxicity in two types of cell lines (A549 and Hep3B) and zebrafish embryos with less than 5 mg mL^{-1} concentration of AC-paints-O. The role of AC-paints-O is first to provide a high quantum yield, thereby penetrating the cell membrane and instigating antibacterial reactions by ROS generation, which can be observed from electron spin resonance spectroscopy (ESR). The resultant ROS will be *in situ* produced during the oxygen atmospheric plasma reaction. The designed AC-paints have excellent biocompatibility, strong fluorescence and unique antibacterial effects. This method opens up a new route to improve C-dots in an easy way and on a large scale.

Experimental

Materials

Polyethylene glycol (PEG) (average M_n = 300) was purchased from Aldrich and used as the source of C-paints and AC-paints.[20]

Atmospheric plasma system

A plasma treatment system (Covance-MP; Femto-Science Co., Korea) consisting of a 13.56 MHz-radio-frequency (RF) generator (up to 300 W), an electrode, dielectric materials, a ceramic substrate, a diffuser, a sample stage (size: 150 × 150 mm), a gas inlet/outlet, and a vacuum system was used. Argon (50 sccm) and oxygen or nitrogen (50 sccm) were employed as the carrier gas and reactive gas, respectively (plasma power: 200 W and time: 30 min).

Morphology

The morphological structure and size of the C-paints and AC-paints were analysed by transmittance electron microscopy (TEM, JEM 2011) and atomic force microscopy (AFM, Digital Instruments: Nanoscope Multimode IV). The TEM specimens were prepared by drop-casting 10 μL of the C-paints and AC-paints solution on a 300 mesh carbon-coated copper TEM grid with a carbon film, followed by drying at room temperature. Drops of dilute aqueous solution (1/2 dilution) of the C-paints and AC-paints were deposited on silicon substrates for AFM. The corresponding particle-size-distribution histogram of the C-paints and AC-paints was plotted using the Lince 2.31d software.

Characterization

AC-paints were characterized using X-ray photoelectron spectroscopy (XPS, Kratos Analytical, AXIS Nova, UK). The Fourier transform infrared (FTIR) spectra were obtained on a FTIR spectrophotometer (FTIR4100/Jasco). UV/Vis absorption spectra were measured by a UV–Vis-NIR spectrophotometer (Varian, Cary 5000, Australia). Fluorescence (FL) spectra were recorded using a UV transilluminator (DUT-260; Core Bio System, Korea) to measure the optical properties of C-paints and AC-paints. The excitation wavelengths were 290–550 nm.

QY measurements

The internal quantum yield was analysed using the quantum yield system (K-MAC, Fluoro-Q2100) at 410 nm excitation using the following equation:

$$\text{Quantum yield} = E_c/(L_a - L_c) \quad (1)$$

Table 1 Information of functionalized C-dots *via* various synthetic and functionalized methods

Preparation method	Surface functionalization	Precursors	Passivation agent	Doping element	Synthesis reaction conditions	Surface reaction conditions	Ref.
Hydrothermal carbonization		Chitosan	—	Amino	180 °C		40
Laser ablation	Thermal treatment	Carbon soot	PEG	Nitrogen	900 °C	110 °C	42
Hydrothermal treatment		Milk	Diamine-terminated oligomeric PEG	Nitrogen	180 °C		43
Hydrothermal treatment	Hydrolyzation and co-condensation	AEAPMS	Silica	Organosilane	240 °C	—	41
Hydrothermal treatment		PEI		Amino	<200 °C		44
Ultrasound irradiation	Atmospheric plasma treatment	PEG	—	Oxygen Nitrogen	Room tem.	Room tem. Gas injection (O_2 and N_2)	This paper

where E_c is the emission processed by direct excitation light, L_a is the total amount of excitation light and L_c is the amount of light after direct excitation.[45]

ESR measurements

For free-radical detection by 5,5-dimethyl-1-pyrroline *N*-oxide (DMPO; 0.3 M in PBS buffer at pH 7.2, Sigma-Aldrich, USA) as a spin-trap agent, an aliquot of the as-prepared samples (C-paints and AC-paints were mixed with DMPO solution) was filled into a capillary tube and directly irradiated with light (>400 nm) from a light-emitting diode (LED) source for 5 min, and the results were recorded *via* ESR spectrometry (JEOL JES-FA200, Japan; centre field: 327 mT; power: 1 mW; amplitude: 5.0 × 100; modulation width: 0.4 × 1; sweep width: 1 × 10; sweep time: 30 s).

ATP assays

ATP assay was performed using a CellTiter-Glo assay kit (Promega Corp., USA) according to the manufacturer's instructions. Briefly, cells from the human bronchial epithelial cell line (BEAS2B), normal adult liver epithelial cell line (THLE2) (1.5×10^4 cells in 100 μL medium per well), adenocarcinomic human alveolar basal epithelial cell line (A549) and human hepatoma cell line (hep3B) (20 000 cells in 100 μL medium per well) were cultured overnight in an opaque-walled 96-well plate and treated with 0–10 mg (serial two-fold dilutions) of C-paints and AC-paints in medium containing 1% FBS. After 24 hours of incubation, assay buffer was added to each well. The plates were agitated for 2 min, followed by incubation for 10 min. Finally, the signal was measured using the GloMax 96 Microplate Luminometer (Promega Corp., USA).

Zebrafish developmental toxicity assays

Zebrafish (wild-type AB line) were maintained at a temperature of 28.5 °C and exposed to 14 h light : 10 h darkness cycles. The embryos were obtained from natural spawning of wild-type adults and cultured at 28.5 °C in egg water. The developmental stage of the embryos was measured according to the standard procedure.[46] This protocol was approved by the Korea Institute of Toxicology (KIT) Institutional Animal Care and Use Committee, and all of the experiments were performed in accordance with the guidelines of the Animal Care Ethics Committee of KIT. The AC-paints developmental toxicity assay included six experimental groups (0.1, 0.5, 1, 5, 10, 50 mg mL^{-1}). Ten fertilized healthy embryos were transferred to a 12-well plate along with 2 mL of E3 medium. The embryos were treated with C-paints and AC-paints suspended in the E3 medium and incubated at 28.5 °C until 96 hpf. The C-paints or AC-paints was replaced with a fresh medium every day during the entire exposure period of 93 h. The morphological malformations (*e.g.*, malformed yolk sacs, tail malformations, delayed development, and oedema in the heart and body cavity) and hatching rates of the larvae were observed and recorded by stereomicroscopy (Nikon, Japan) along with a digital camera.

Bio-imaging

HeLa cells were seeded in Dulbecco's Modified Eagle Medium (DMEM) containing glucose supplemented with 10% FBS, 100 units per mL penicillin, and 100 mg per mL streptomycin. When the HeLa cells were grown in stationary phase, the cells (~2×10^5 cell per mL) were dispersed within replicate 6-well plates to a total volume of 2 mL per well and maintained at 37 °C in a 5% CO_2 incubator for 24 h. The culture medium was then removed, and the cells were incubated in the culture medium containing C-paints and AC-paints for 24 h, followed by washing with the culture medium. Fluorescence images were obtained using a confocal microscope (LSM 510META; Carl Zeiss).

Antimicrobial activity

Escherichia coli (DH5α) and *Acinetobacter baumannii* (DU202) were used for the bacterial experiments. Bacteria were grown at 37 °C in Luria–Bertani (LB) broth (Difco, Sparks, MD, USA) with continuous shaking. Various concentrations of AC-paints were applied to the bacterial culture, and the bacterial growth was measured using a UV spectrophotometer at an optical density of 600 nm (OD600) at 2-hour intervals for 12 hours. Intracellular oxidation levels of the bacteria were measured using the oxidant-sensitive probe H2DCFDA (general oxidative stress indicator, ThermoFisher Scientific C6827). *E. coli* DH5α cells were grown until OD600 0.4 and either left untreated or were treated with 20 μg mL^{-1} of C-paints, AC-paints (O_2 and N_2), or 50 μM of H_2O_2 for 2 hours. The cells were washed with 10 mM potassium phosphate buffer, pH 7.0, and incubated for 30 min in the same buffer with 10 μM H2DCFDA dissolved in dimethyl sulphoxide. The cells were washed and extracted *via* sonication. The cell extracts (100 μL) were mixed with 1 mL of phosphate buffer (pH 7.0), and the fluorescence intensity was measured at 2 min intervals for 20 min. The emission values were normalized by protein concentration. The *E. coli* treated with AC-paints for 12 h was fixed with 2.5% glutaraldehyde and examined under the Energy Filtering Transmission Electron Microscope (Libra 120).

Results and discussion

Synthesis and characterization of AC-paints

In a typical preparation, the C-paints were synthesized according to a method reported previously.[20] After cooling, the as-prepared C-paints were subjected to plasma treatment to introduce functional groups on the surface of C-paints to fabricate AC-paints; the synthesis route is briefly illustrated in Scheme 1. Herein, the AC-paints are small carbon nanoparticles that are surface-functionalized with re-deposited organic molecules and/or active species by atmospheric plasma treatment. Three major purposes were achieved *via* plasma treatment of AC-paints: (1) generation of bright luminescence, (2) improvement of hydrophilicity and stability, and (3) surface functionalization of AC-paints for antibacterial activity. The morphology, structure, and composition of

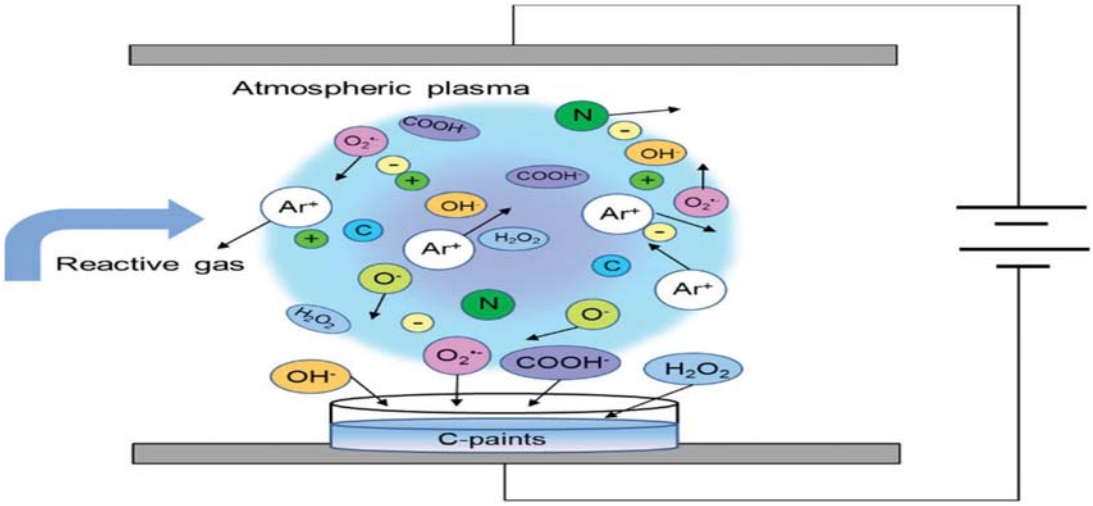

Scheme 1 Schematic of plasma reaction with C-paints. Atmospheric plasma treatment resulted in the formation of functional groups on the surface of C-paints to fabricate AC-paints. On addition of reactive gases involving oxygen or nitrogen, organic molecules or reactive oxygen species were formed on the surface of C-paints.

AC-paints were characterized by transmission electron microscopy (TEM), atomic force microscopy (AFM), X-ray photoelectron spectroscopy (XPS) and Fourier transform infrared (FTIR) spectroscopy.

TEM and AFM images of C-paints and AC-paints confirmed the formation of well-dispersed and spherical particles with a size in the range of 2.3–6.3 nm (average 3.77 nm), as shown in Fig. 1A and Fig. S2;† in addition, several amorphous structures were also observed in the images. As depicted in Fig. S1,† AC-paints maintained a spherical morphology and no topographic differences were revealed compared with C-paints. XPS results indicated that the C-paints and AC-paints mainly contained carbon and oxygen, but nitrogen plasma-treated AC-paints-N had a low nitrogen content. As shown in Fig. 1B, the spectra of C-paints and AC-paints possess two typical peaks of the C 1s (285 eV), O 1s (531 eV), and a lower peak of N 1s (400 eV). After plasma (O_2 and N_2) treatment, the oxygen content increased. After N_2 plasma treatment, a distinct increase in the nitrogen content was observed (Table S1†). These changes were also confirmed by FTIR. In FTIR spectra, AC-paints-O showed an increase in absorption of O–H stretching at 3448 cm^{-1} and AC-paints-N exhibited the absorption bands at around 3440, 1120, and 810 cm^{-1}, corresponding to N–H stretching and C–N bond vibrations compared with C-paints (Fig. S3†).[47,48]

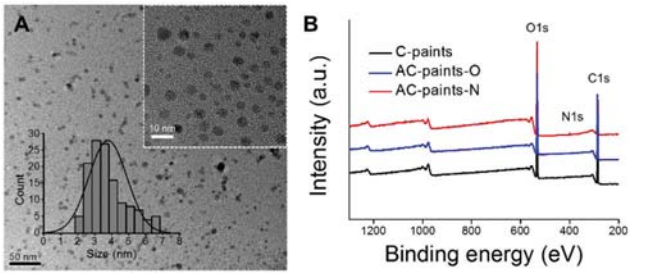

Fig. 1 Characterization of C-paints and AC-paints. (A) TEM images of AC-paints-O after oxygen plasma treatment of C-paints. Inset shows size distribution of AC-paints-O, (B) XPS spectra of C-paints and AC-paints (O_2 and N_2).

Photoluminescence properties and identification of reactive oxygen species of AC-paints

The optical properties of AC-paints were measured to reveal the effect of atmospheric plasma on fluorescence (FL) behaviours. Fig. S4† shows the absorption spectrum with a strong peak at 245 nm, which indicates the presence of C=C group of C-paints and AC-paints. In Fig. 2A, the AC-paints showed broad absorbance from the UV to the visible region and strong emission in the visible region (400–700 nm), and the maximum excitation and emission wavelengths of the C-paints and AC-paints were located at 410 and 500 nm, respectively

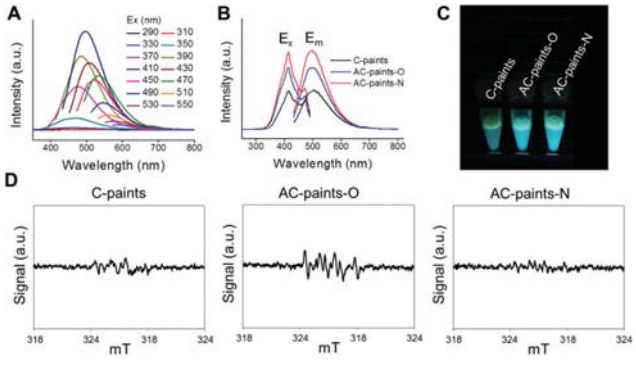

Fig. 2 Optical properties of C-paints and AC-paints. Fluorescence spectra of (A) AC-paints-O and (B) excitation (E_x) and emission (E_m) of C-paints and AC-paints, (C) photograph of C-paints and AC-paints under UV light (360 nm) and (D) electron spin resonance spectra of C-paints and AC-paints (O_2 and N_2) under LED light (>400 nm).

(Fig. 2B). It was revealed that the FL intensities of AC-paints significantly increased compared with those of C-paints and the photograph showed fluorescence difference under a hand-held UV lamp, as shown in Fig. 2C. The intensity of fluorescence of AC-paints reflects the effect of surface functional groups on C-paints *via* atmospheric plasma treatment. The plasma-induced doping or functionalization introduces a new type of surface functional groups on C-paints such as carboxyl, hydroxyl or amine groups, which plays a key role in enhancing the optical behaviour by filling defects on the surface of C-dot.[7,49–51] Moreover, the strongest fluorescence was observed for AC-paints-N at 410 nm excitation because N_2 gas-injected plasma could be attributed to the presence of N-containing groups on the surface. According to XPS and FTIR, AC-paints-N have specific groups including amine as well as hydroxyl groups. As the samples could emit maximum fluorescence when excited at 410 nm, the relative fluorescence quantum yields of C-paints and AC-paints-O excited with 401–419 nm visible light were calculated to be 6.1 and 12.0, respectively. The surface-functionalized AC-paints exhibited quantum yields two times higher than C-paints.

To investigate the molecular oxygen activation of C-paints and AC-paints, we monitored ROS generation using electron spin resonance (ESR) techniques. ROS can damage the DNA, cell membranes and cellular proteins and may lead to cell death. The hydroxyl radical ($^{\bullet}OH$) is the most known reactive oxygen radical, and it reacts very quickly with almost every type of molecule found in living cells. We therefore evaluated the antibacterial activities of C-paints and AC-paints by determining the ROS intensity. In Fig. 2D, we found that the ESR signal was observed for C-paints and AC-paints with various gases (O_2 and N_2 in plasma processing) owing to the functional groups on their surfaces. Compared with C-paints, the ESR signals revealed increased ROS levels on AC-paints after exposure to the O_2 plasma. These results indicate that $O_2^{\bullet-}$ and $^{\bullet}OH$ radicals were produced through reaction with the O_2 plasma. We selected O_2 plasma-treated AC-paints (AC-paints-O) as the antibacterial model.

Cytotoxicity, developmental toxicity and bio-imaging of AC-paints

Dose-dependent cell viability was determined in four types of cells including BEAS2B, THLE2, A549 and hep3B, which were chosen to represent the normal lung cell, normal hepatocytes, lung carcinoma and liver hepatocytes, respectively (Fig. 3). We chose the adenosine triphosphate (ATP) measurement method for AC-paints because the conventional viability assays based on colorimetric measurements, such as acid phosphatase (APH) and methyl tetrazolium (MTT) assay, could be affected by nanoparticles featuring broad absorption spectra. Moreover, high concentrations of AC-paints can interfere with the signals, thus causing false positive results as well as distorted data. This assay is a luminescence-based method of determining the number of viable cells in a culture based on the quantification of ATP present, which signals the presence of metabolically active cells. Targeted cells were treated with a

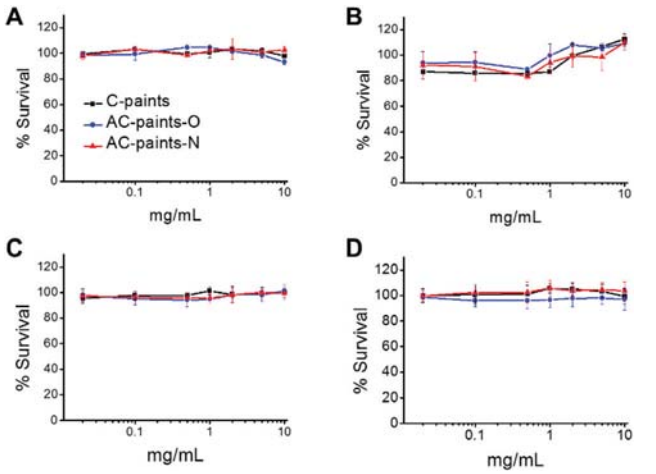

Fig. 3 *In vitro* cytotoxicity of C-paints and AC-paints (A) BEAS2B lung cell, (B) THLE2 hepatocyte, (C) A549 lung carcinoma and (D) Hep3B hepatocyte.

wide range of doses (0.02 to 10 mg mL^{-1}) of AC-paints for 24 hours. Our results showed that the C-paints and AC-paints exhibit low cytotoxicity to a concentration of ~10 mg mL^{-1} AC-paints for 4 cell lines. These results demonstrated that the C-paints and AC-paints can be used for various biological purposes.

Before further using the AC-paints for biological studies, we tested the developmental toxicity of C-paints and AC-paints using zebrafish embryos after exposure to the as-synthesized AC-paints. Zebrafish embryos were exposed to the AC-paints, starting at 3 h post-fertilization (hpf) and analysed every 24 h up to 96 hpf. Fig. 4A shows images of entire bodies of zebrafish larvae after exposure to AC-paints at different concentrations for 93 h, demonstrating that the AC-paints were successfully introduced into the larvae from samples with concentrations ranging from 100 μg mL^{-1} to 50 mg mL^{-1}. Fig. 4B and C show that the delay in hatching of larvae treated with AC-paint solutions is similar to that of the control group for 28 hpf, and the zebrafish larvae grew normally after 72 hpf except when exposed to a high concentration of AC-paints-O (>5 mg mL^{-1}). As shown in Fig. 5A and C, the developmental toxic effects were negligible for AC-paints (O_2 and N_2); the hatching rate of zebrafish embryos was higher than 90% with exposure to 10 mg mL^{-1} of AC-paints during 72–96 hpf, whereas the hatching rate decreased to about 7.5 ± 2.4% with 10 mg mL^{-1} of AC-paints-O. Zebrafish hatching is an essential step in their development and survival. Delayed hatching can arrest embryonic development and maturation, leading to eventual death within the chorion. Zebrafish can be used as a vertebrate model organism because it has similar gene sequences and organ systems to human beings.

Fig. 6 shows confocal images of immortal cell lines (HeLa) treated with C-paints. From these images, it can be observed that the blue and green fluorescent emissions are mainly located in the cytoplasm, suggesting that C-paints and AC-paints can pass through cell membranes and enter cells.

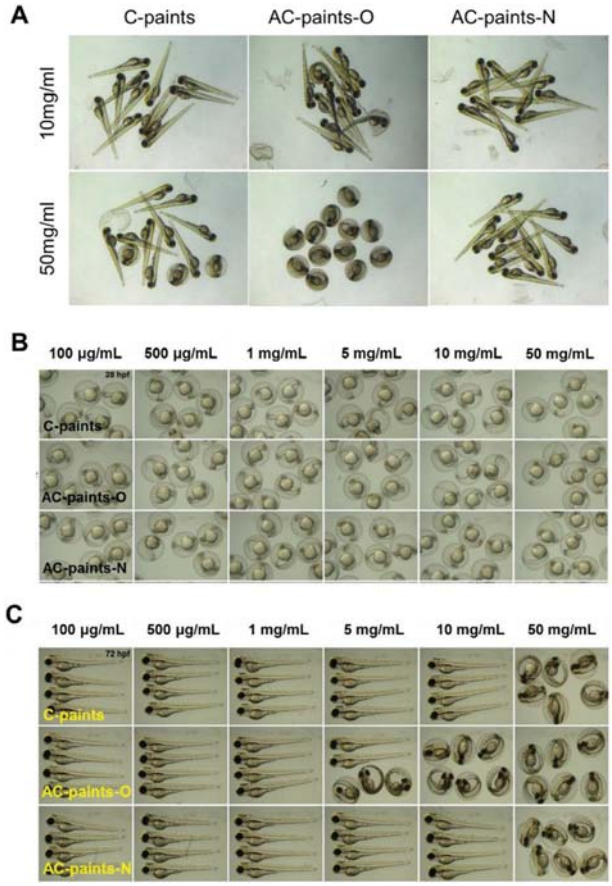

Fig. 4 Developmental toxicity of C-paints and AC-paints. (A) Representative micrographs of zebrafish hatching larvae at 72 hpf. Zebrafish exposed to 10 and 50 mg mL^{-1} of AC-paints (O_2 and N_2 plasma treated). Images of zebrafish embryos at (B) 28 hpf and (C) 72 hpf after treatment of C-paints and AC-paints (O_2 and N_2) with different concentrations.

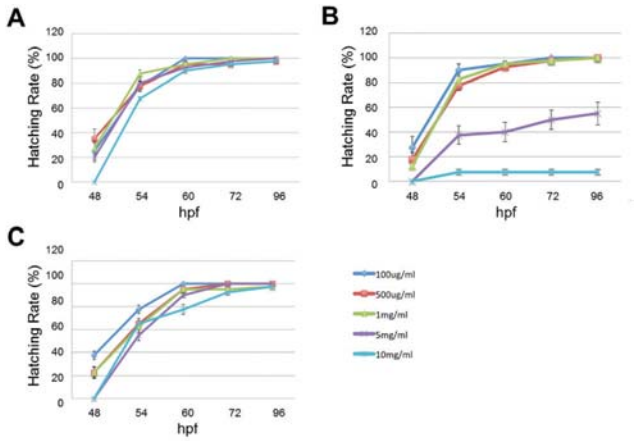

Fig. 5 Zebrafish exposed to 10 and 50 mg mL^{-1} of AC-paints (O_2 and N_2 plasma treated). Developmental toxicity of (A) C-paints, (B) AC-paints-O and (C) AC-paints-N.

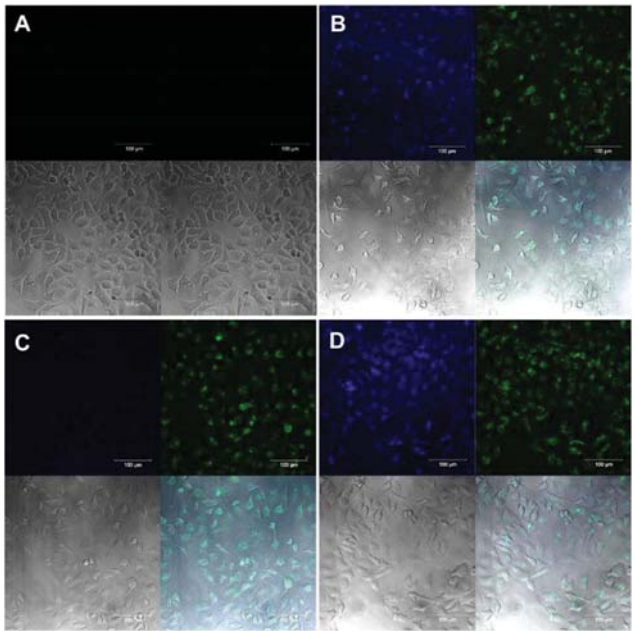

Fig. 6 Confocal fluorescence images of (A) control, (B) C-paints, (C) AC-paints-O and (D) AC-paints-N in HeLa cells, bright field and merged images, respectively.

Considering their low developmental toxicity in zebrafish and enhanced fluorescent properties, the as-obtained AC-paints might be promising bio-imaging reagents.

Antibacterial behaviour of AC-paints

Gram-negative *Escherichia coli* (*E. coli*) and multi-drug-resistant *Acinetobacter baumannii* (*A. baumannii*) were used as model bacteria to evaluate the antibacterial activities of C-paints and AC-paints (Fig. 7 and 8). The samples were applied to bacterial culture media at various concentrations, and the bacterial growth was determined by measuring the optical density of the sample measured at a wavelength of 600 nm (OD600). The results showed that C-paints and AC-paints inhibited *E. coli* growth in a dose-dependent manner at low concentrations of AC-paints (>1 mg mL^{-1}) (Fig. 7A). We further examined the antibacterial activity of AC-paints using the multi-drug-resistant bacteria. C-paints and AC-paints also effectively inhibited the growth of the multi-drug-resistant bacteria *A. baumannii* at low concentrations of AC-paints (>1 mg mL^{-1}) (Fig. 7B). To investigate the antibacterial mechanism of AC-paints, the cytoplasmic ROS content was measured in *E. coli*. The ROS monitoring was achieved using the oxidant-sensitive probe dichlorodihydrofluorescein diacetate (H2DCFDA), which indicated increased ROS levels in *E. coli* after exposure to AC-paints. This showed that cytoplasmic ROS was elevated by the treatment with AC-paints. As shown in Fig. 7C, two samples marked untreated and H_2O_2 were used as negative and positive controls, respectively. The endogenous ROS generation induced by AC-paints was higher than that in the untreated sample. These results reveal that AC-paints may kill bacteria by generating

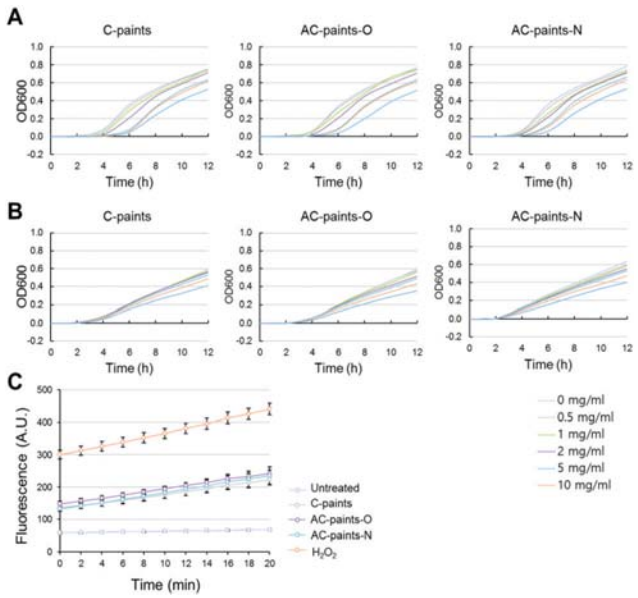

Fig. 7 Antibacterial activity of C-paints and AC-paints. Optical density at 600 nm (OD600) of bacterial suspension of (A) *E. coli* and (B) *A. baumannii* with different concentration of C-paints or AC-paints, (C) cytoplasmic ROS content was evaluated measuring the H2DCFDA probe activation in *E. coli* cells treated with indicated substrates.

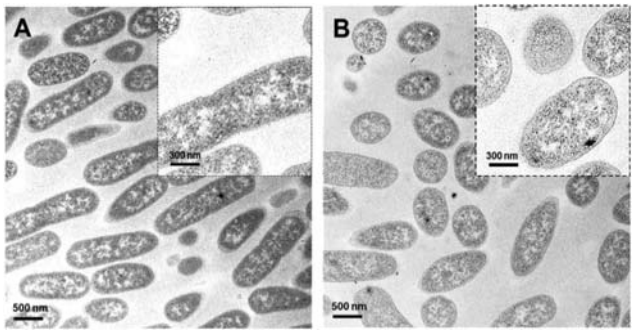

Fig. 8 TEM images of *E. coli* as control (A) and *E. coli* exposed to AC-paints-O at 37 °C for 12 h (B).

ROS. During interaction with the O_2 plasma, electrons and radicals produce ROS that are known to kill bacteria. The generation of ROS induced by plasma depends on the presence of atmospheric oxygen and moisture during the plasma reaction. The generated ROS can oxidize the phospholipids integral to the membrane structure and is likely the major factor inhibiting bacterial growth.

To confirm the changes in bacterial morphology induced by the antibacterial system, TEM was used to observe *E. coli* after injection of AC-paints-O. The hydrophilic AC-paints-O have excellent solubility in water and various organic solvents, and they can penetrate the membrane and subsequently oxidize the cell contents *via* ROS. As shown in Fig. 8, untreated *E. coli* cells were typically rod-shaped with smooth and unbroken cell walls. The bacterial surface became rough and wrinkled after exposure to AC-paints-O since ROS could oxidize the lipid membrane and destroy the bacterial membranes.

Conclusions

In summary, we used atmospheric plasma treatment as a surface functionalization method to enhance the optical properties and antibacterial activities of the as-synthesized C-dots (AC-paints). The significantly enhanced fluorescence of AC-paints compared with C-paints in previous reports is assumed to originate from the production of functional groups *via* plasma treatment. We investigated the toxicity of the atmospheric plasma (O_2 and N_2)-treated AC-paints on BEAS2B, THLE2, A549 and hep3B *in vitro* and no significant cytotoxic effect of AC-paints on zebrafish *in vivo* was observed. Owing to their strong fluorescence and low cytotoxicity, the AC-paints can be used as bio-imaging agents with blue and green fluorescence. We have extended the use of AC-paints as antibacterial materials and the antibacterial properties of AC-paints towards *E. coli* bacterial cells were also studied. We suggested that the antibacterial activity of AC-paints at low concentrations (>1 mg mL^{-1}) is a result of ROS production by plasma, which was supported by ESR measurements. In this study, new insights into the antibacterial effects of the C-dots have been provided. We anticipate that the AC-paints can be utilized for the replacement of metal-based fluorescent nanomaterials in biomedicine and environmental applications.

Acknowledgements

This study was supported by the Korea Basic Science Institute (KBSI) research under Grant No. E37800 and K36327.

Notes and references

1 H. Gao, A. V. Sapelkin, M. M. Titirici and G. B. Sukhorukov, *ACS Nano*, 2016, **10**, 9608.
2 Y. Dong, H. Pang, H. Bin Yang, C. Guo, J. Shao, Y. Chi, C. M. Li and T. Yu, *Angew. Chem., Int. Ed.*, 2013, **52**, 7800.
3 S. Zhu, Q. Meng, L. Wang, J. Zhang, Y. Song, H. Jin, K. Zhang, H. Sun, H. Wang and B. Yang, *Angew. Chem., Int. Ed.*, 2013, **52**, 3953.
4 Y. Fang, S. Guo, D. Li, C. Zhu, W. Ren, S. Dong and E. Wang, *ACS Nano*, 2011, **6**, 400.
5 C. Shih, P. Chen, G. Lin, C. Wang and H. Chang, *ACS Nano*, 2015, **9**, 312.
6 H. Ding, S.-B. Yu, J.-S. Wei and H.-M. Xiong, *ACS Nano*, 2016, **10**, 484.
7 X. Li, M. Rui, J. Song, Z. Shen and H. Zeng, *Adv. Funct. Mater.*, 2015, **25**, 4929.
8 H. Hou, C. E. Banks, M. Jing, Y. Zhang and X. Ji, *Adv. Mater.*, 2015, **27**, 7861.
9 S. L. D'souza, B. Deshmukh, K. A. Rawat, J. R. Bhamore, N. Lenka and S. K. Kailasa, *New J. Chem.*, 2016, **40**, 7075.

10 V. N. Mehta, S. Jha, H. Basu, R. K. Singhal and S. K. Kailasa, *Sens. Actuat. B*, 2015, **213**, 434.
11 C. Wu and D. T. Chiu, *Angew. Chem., Int. Ed.*, 2013, **52**, 3086.
12 Y.-F. Wu, H.-C. Wu, C.-H. Kuan, C.-J. Lin, L.-W. Wang, C.-W. Chang and T.-W. Wang, *Sci. Rep.*, 2016, **6**, 21170.
13 T. Feng, X. Ai, G. An, P. Yang and Y. Zhao, *ACS Nano*, 2016, **10**, 4410.
14 A. B. Bourlinos, A. Stassinopoulos, D. Anglos, R. Zboril, M. Karakassides and E. P. Giannelis, *Small*, 2008, **4**, 455.
15 X. T. Zheng, A. Ananthanarayanan, K. Q. Luo and P. Chen, *Small*, 2015, **11**, 1620.
16 K. Jiang, S. Sun, L. Zhang, Y. Lu, A. Wu, C. Cai and H. Lin, *Angew. Chem., Int. Ed.*, 2015, **54**, 5360.
17 V. N. Mehta, S. Jha and S. K. Kailasa, *Mater. Sci. Eng. C*, 2014, **38**, 20.
18 V. N. Mehta, S. Jha, R. K. Singhal and S. K. Kailasa, *New. J. Chem.*, 2014, **38**, 6152.
19 W. Wei, C. Xu, L. Wu, J. Wang, J. Ren and X. Qu, *Sci. Rep.*, 2014, **4**, 3564.
20 S. Y. Park, H. U. Lee, Y.-C. Lee, S. Choi, D. H. Cho, H. S. Kim, S. Bang, S. Seo, S. C. Lee, J. Won, B.-C. Son, M. Yang and J. Lee, *Sci. Rep.*, 2015, **5**, 12420.
21 H. U. Lee, S. Y. Park, E. S. Park, B. Son, S. C. Lee, J. W. Lee, Y.-C. Lee, K. S. Kang, M. Il Kim, H. G. Park, S. Choi, Y. S. Huh, S.-Y. Lee, K.-B. Lee, Y.-K. Oh and J. Lee, *Sci. Rep.*, 2014, **4**, 4665.
22 S. Y. Park, H. U. Lee, E. S. Park, S. C. Lee, J.-W. Lee, S. W. Jeong, C. H. Kim, Y.-C. Lee, Y. S. Huh and J. Lee, *ACS Appl. Mater. Interfaces*, 2014, **6**, 3365.
23 Z. Zhang, J. Zhang, B. Zhang and J. Tang, *Nanoscale*, 2013, **5**, 118.
24 J. Fei, J. Zhao, C. Du, A. Wang, H. Zhang, L. Dai and J. Li, *ACS Nano*, 2014, **8**, 8529.
25 W. Yin, J. Yu, F. Lv, L. Yan, L. R. Zheng, Z. Gu and Y. Zhao, *ACS Nano*, 2016, **10**, 11000.
26 R. Li, N. D. Mansukhani, L. M. Guiney, Z. Ji, Y. Zhao, C. H. Chang, C. T. French, J. F. Miller, M. C. Hersam, A. E. Nel and T. Xia, *ACS Nano*, 2016, **10**, 10966.
27 I. N. Kholmanov, M. D. Stoller, J. Edgeworth, W. H. Lee, H. Li, J. Lee, C. Barnhart, J. R. Potts, R. Piner, D. Akinwande, J. E. Barrick and R. S. Ruoff, *ACS Nano*, 2012, **6**, 5157.
28 M. Wu, B. Ma, T. Pan, S. Chen and J. Sun, *Adv. Funct. Mater.*, 2016, **26**, 569.
29 Z. Xiu, Q. Zhang, H. L. Puppala, V. L. Colvin and P. J. J. Alvarez, *Nano Lett.*, 2012, **12**, 4271.
30 J. Wang, J. Li, S. Qian, G. Guo, Q. Wang, J. Tang, H. Shen, X. Liu, X. Zhang and P. K. Chu, *ACS Appl. Mater. Interfaces*, 2016, **8**, 11162.
31 J. Xu, X. Zhou, Z. Gao, Y. Y. Song and P. Schmuki, *Angew. Chem., Int. Ed.*, 2016, **55**, 593.
32 S. Liu, T. H. Zeng, M. Hofmann, E. Burcombe, J. Wei, R. Jiang, J. Kong and Y. Chen, *ACS Nano*, 2011, **5**, 6971.
33 W. Hu, C. Peng, W. Luo, M. Lv, X. Li, D. Li, Q. Huang and C. Fan, *ACS Nano*, 2010, **4**, 4317.
34 J. Zhao, B. Deng, M. Lv, J. Li, Y. Zhang, H. Jiang, C. Peng, J. Li, J. Shi, Q. Huang and C. Fan, *Adv. Healthcare Mater.*, 2013, **2**, 1259.
35 H. Chen, B. Wang, D. Gao, M. Guan, L. Zheng, H. Ouyang, Z. Chai, Y. Zhao and W. Feng, *Small*, 2013, **9**, 2735.
36 C. Li, S. Bolisetty, K. Chaitanya, J. Adamcik and R. Mezzenga, *Adv. Mater.*, 2013, **25**, 1010.
37 S. Qu, X. Wang, Q. Lu, X. Liu and L. Wang, *Angew. Chem., Int. Ed.*, 2012, **51**, 12215.
38 M. Zheng, S. Liu, J. Li, D. Qu, H. Zhao, X. Guan, X. Hu, Z. Xie, X. Jing and Z. Sun, *Adv. Mater.*, 2014, **26**, 3554.
39 H. Wang, J. Di, Y. Sun, J. Fu, Z. Wei, H. Matsui, A. D. C. Alonso and S. Zhou, *Adv. Funct. Mater.*, 2015, **25**, 5537.
40 Y. Yang, J. Cui, M. Zheng, C. Hu, S. Tan, Y. Xiao, Q. Yang and Y. Liu, *Chem. Commun.*, 2012, **48**, 380.
41 F. Wang, Z. Xie, H. Zhang, C. Liu and Y.-g. Zhang, *Adv. Funct. Mater.*, 2011, **21**, 1027.
42 X. Wang, L. Cao, S.-T. Yang, F. Lu, M. J. Meziani, L. Tian, K. W. Sun, M. A. Bloodgood and Y.-P. Sun, *Angew. Chem., Int. Ed.*, 2010, **122**, 5438.
43 L. Wang and H. S. Zhou, *Anal. Chem.*, 2014, **86**, 8902.
44 Y. Dong, R. Wang, H. Li, J. Shao, Y. Chi, X. Lin and G. Chen, *Carbon*, 2012, **50**, 2810.
45 P.-Y. Lin, C.-W. Hsieh, M.-L. Kung, L.-Y. Chua, H.-J. Huang, H.-T. Chen, D.-C. Wu, C.-H. Kuo, S.-L. Hsieh and S. Hsieh, *J. Biotech.*, 2014, **189**, 114.
46 M. Westerfield, *The Zebrafish Book: A Guide for the Laboratory Use of Zebrafish (Danio rerio)*, Univ. of Oregon Press, Eugene, 5th edn, 2007.
47 H. Ding, J.-S. Wei and H.-M. Xiong, *Nanoscale*, 2014, **6**, 13817.
48 Y. V. Panasiuk, A. E. Raevskaya, O. L. Stroyuk, P. M. Lytvyn and S. Y. Kuchmiy, *RSC Adv.*, 2015, **5**, 46843.
49 P. Anilkumar, L. Cao, J.-J. Yu, K. N. Tackett, P. Wang, M. J. Meziani and Y.-P. Sun, *Small*, 2013, **9**, 545.
50 S. C. Ray, A. Saha, N. R. Jana and R. Sarkar, *J. Phys. Chem. C*, 2009, **113**, 18546.
51 K. Hola, Y. Zhang, Y. Wang, E. P. Giannelis, R. Zboril and A. L. Rogach, *Nano Today*, 2014, **9**, 590.

